

# Spin Injection and Nonlocal Spin Transport in Magnetic Nanostructures

S. Takahashi and S. Maekawa

*Institute for Materials Research, Tohoku University, Sendai 980-8577, Japan,  
and CREST, Japan Science and Technology Corporation, Kawaguchi 332-0012, Japan*

(Dated: September 1, 2005)

We theoretically study the nonlocal spin transport in a device consisting of a nonmagnetic metal (N) and ferromagnetic injector (F1) and detector (F2) electrodes connected to N. We solve the spin-dependent transport equations in a device with arbitrary interface resistance from a metallic-contact to tunneling regime, and obtain the conditions for efficient spin injection, accumulation, and transport in the device. In a device containing a superconductor (F1/S/F2), the effect of superconductivity on the spin transport is investigated. The spin-current induced spin Hall effect in nonmagnetic metals is also discussed.

PACS numbers:

## 1. Introduction

There has been considerable interest in spin transport in magnetic nanostructures, because of their potential applications as spin-electronic devices [1]. The spin polarized electrons injected from a ferromagnet (F) into a nonmagnetic material (N) such as a normal metal, semiconductor, and superconductor create a nonequilibrium spin accumulation in N. The efficient spin injection, accumulation, and transport are central issues for utilizing the spin degree of freedom as in spin-electronic devices. It has been demonstrated that the injected spins penetrate into N over the spin-diffusion length ( $l_N$ ) of the order of  $1\ \mu\text{m}$  using spin injection and detection technique in F1/N/F2 trilayer structures (F1 is an injector and F2 a detector) [2]. Recently, several groups have succeeded in observing spin accumulation by the *nonlocal* spin injection and detection technique [3, 4, 5, 6, 7, 8, 9].

In this paper, we study the spin accumulation and spin current, and their detection in the nonlocal geometry of a F1/N/F2 nanostructure. We solve the diffusive transport equations for the electrochemical potential (ECP) for up and down spins in the structure of arbitrary interface resistances ranging from a metallic-contact to a tunneling regime, and examine the optimal conditions for spin accumulation and spin current. Efficient spin injection and detection are achieved when a tunnel barrier is inserted at the interface, whereas a large spin-current injection from N into F2 is realized when N is in metallic contact with F2, because F2 plays the role of strong spin absorber. In a tunnel device containing a superconductor (F1/S/F2), the effect of superconductivity on the spin transport is discussed. The spin-current induced anomalous Hall effect is also discussed.

## 2. Spin injection and accumulation

We consider a spin injection and detection device consisting of a nonmagnetic metal N connected to ferromagnetic injector F1 and detector F2 as shown in Fig. 1. The

F1 and F2 are the same ferromagnets of width  $w_F$  and thickness  $d_F$  and are separated by distance  $L$ , and N of width  $w_N$  and thickness  $d_N$ . The magnetizations of F1 and F2 are aligned either parallel or antiparallel.

In the diffusive spin transport, the current  $\mathbf{j}^\sigma$  for spin channel  $\sigma$  in the electrodes is driven by the gradient of ECP ( $\mu^\sigma$ ) according to  $\mathbf{j}^\sigma = -(1/e\rho^\sigma)\nabla\mu^\sigma$ , where  $\rho^\sigma$  is the resistivity. The continuity equations for the charge and spin currents in a steady state yield [2, 11, 12, 13, 14]

$$\nabla^2 (\mu^\uparrow/\rho^\uparrow + \mu^\downarrow/\rho^\downarrow) = 0, \quad (1)$$

$$\nabla^2 (\mu^\uparrow - \mu^\downarrow) = l^{-2} (\mu^\uparrow - \mu^\downarrow), \quad (2)$$

where  $l$  is the spin-diffusion length and takes  $l_N$  in N and  $l_F$  in F. We note that  $l_N$  ( $l_{\text{Cu}} \sim 1\ \mu\text{m}$  [3],  $l_{\text{Al}} \sim 1\ \mu\text{m}$  [2, 4]) is much larger than  $l_F$  ( $l_{\text{Py}} \sim 5\ \text{nm}$ ,  $l_{\text{CoFe}} \sim 12\ \text{nm}$ ,  $l_{\text{Co}} \sim 50\ \text{nm}$ ) [15].

We employ a simple model for the interfacial current across the junctions [11]. Due to the spin-dependent interface resistance  $R_i^\sigma$  ( $i = 1, 2$ ), the ECP is discontinuous at the interface, and the current  $I_i^\sigma$  across the interface

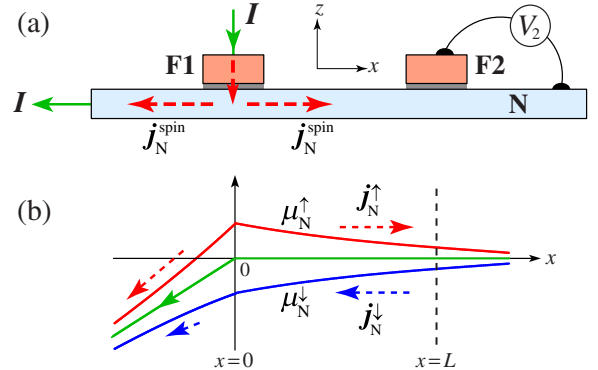


FIG. 1: (a) Spin injection and detection device (side view). The current  $I$  is applied from F1 to the left side of N. The spin accumulation at  $x = L$  is detected by measuring voltage  $V_2$  between F2 and N. (b) Spatial variation of the electrochemical potential (ECP) for up and down spin electrons in N.

( $z = 0$ ) is given by  $I_i^\sigma = (1/eR_i^\sigma)(\mu_F^\sigma|_{z=0^+} - \mu_N^\sigma|_{z=0^-})$ , where the current distribution is assumed to be uniform over the contact area [16, 17]. In a transparent contact (tunnel junction) the discontinuous drop in ECP is much smaller (larger) than the spin splitting of ECP. The interfacial charge and spin currents are  $I_i = I_i^\uparrow + I_i^\downarrow$  and  $I_i^{\text{spin}} = I_i^\uparrow - I_i^\downarrow$ .

When the bias current  $I$  flows from F1 to the left side of N ( $I_1 = I$ ), there is no charge current on the right side ( $I_2 = 0$ ). The solution for Eqs. (1) and (2) takes the form  $\mu_N^\sigma(x) = \bar{\mu}_N + \sigma\delta\mu_N$  with the average  $\bar{\mu}_N = -(eI\rho_N/A_N)x$  for  $x < 0$  and  $\bar{\mu}_N = 0$  for  $x > 0$ , and the splitting  $\delta\mu_N = a_1e^{-|x|/l_N} - a_2e^{-|x-L|/l_N}$ , where the  $a_1$ -term represents the spin accumulation due to spin injection at  $x = 0$ ,

while the  $a_2$ -term the decrease of spin accumulation due to the contact of F2. Note that the pure spin current  $I_N^{\text{spin}} = I_N^\uparrow - I_N^\downarrow$  flows in the region of  $x > 0$ .

In the F1 and F2 electrodes, the solution takes the form  $\mu_{Fi}^\sigma(z) = \bar{\mu}_{Fi} + \sigma b_i(\rho_F^\sigma/\rho_F)e^{-z/l_F}$ , with  $\bar{\mu}_{F1} = -(eI\rho_F/A_J)z + eV_1$  in F1 and  $\bar{\mu}_{F2} = eV_2$  in F2, where  $V_1$  and  $V_2$  are the voltage drops across junctions 1 and 2, and  $A_J = w_N w_F$  is the contact area of the junctions.

Using the matching condition for the spin current at the interfaces, we can determine the constants  $a_i$ ,  $b_i$ , and  $V_i$ . The spin-dependent voltages detected by F2 are  $V_2^P$  and  $V_2^{\text{AP}}$  for the parallel (P) and antiparallel (AP) alignment of magnetizations. The spin accumulation signal detected by F2,  $R_s = (V_2^P - V_2^{\text{AP}})/I$ , is given by [14]

$$R_s = 4R_N \frac{\left(\frac{P_1 R_1}{1 - P_1^2 R_N} + \frac{p_F R_F}{1 - p_F^2 R_N}\right) \left(\frac{P_2 R_2}{1 - P_2^2 R_N} + \frac{p_F R_F}{1 - p_F^2 R_N}\right) e^{-L/l_N}}{\left(1 + \frac{2 R_1}{1 - P_1^2 R_N} + \frac{2 R_F}{1 - p_F^2 R_N}\right) \left(1 + \frac{2 R_2}{1 - P_2^2 R_N} + \frac{2 R_F}{1 - p_F^2 R_N}\right) - e^{-2L/l_N}}, \quad (3)$$

where  $R_N = \rho_N l_N / A_N$  and  $R_F = \rho_F l_F / A_J$  are the *spin-accumulation resistances* of the N and F electrodes,  $A_N = w_N d_N$  is the cross-sectional area of N,  $R_i = R_i^\uparrow + R_i^\downarrow$  is the interface resistance of junction  $i$ ,  $P_i = |R_i^\uparrow - R_i^\downarrow| / R_i$  is the interfacial current spin-polarization, and  $p_F = |\rho_F^\uparrow - \rho_F^\downarrow| / \rho_F$  is the spin-polarization of F. In metallic contact junctions, the spin polarizations,  $P_i$  and  $p_F$ , range around 40–70% from GMR experiments [15] and point-contact Andreev-reflection experiments [18], whereas in tunnel junctions,  $P_i$  ranges around 30–55% from superconducting tunneling spectroscopy experiments with alumina tunnel barriers [19, 20, 21], and  $\sim 85\%$  in MgO barriers [22, 23].

The spin accumulation signal  $R_s$  strongly depends on whether each junction is either a metallic contact or a tunnel junction. By noting that there is large disparity between  $R_N$  and  $R_F$  ( $R_F/R_N \sim 0.01$  for Cu and Py [3]), we have the following limiting cases. When both junctions are transparent contact ( $R_1, R_2 \ll R_F$ ), we have [3, 12, 13]

$$R_s/R_N = \frac{2p_F^2}{(1 - p_F^2)^2} \left(\frac{R_F}{R_N}\right)^2 \sinh^{-1}(L/l_N). \quad (4)$$

When junction 1 is a tunnel junction and junction 2 is a transparent contact (*e.g.*,  $R_2 \ll R_F \ll R_N \ll R_1$ ), we have [14]

$$R_s/R_N = \frac{2p_F P_1}{(1 - p_F^2)} \left(\frac{R_F}{R_N}\right) e^{-L/l_N}. \quad (5)$$

When both junctions are tunnel junctions ( $R_1, R_2 \gg$

$R_N$ ), we have [2, 4]

$$R_s/R_N = P_1 P_2 e^{-L/l_N}, \quad (6)$$

where  $P_T = P_1 = P_2$ . Note that  $R_s$  in the above limiting cases is independent of  $R_i$ .

We compare our theoretical result to experimental data measured by several groups. Figure 2 shows the theoretical curves and the experimental data of  $R_s$  as a function of  $L$ . The solid curves are the values in a tunnel device, and the dashed curves are those in a

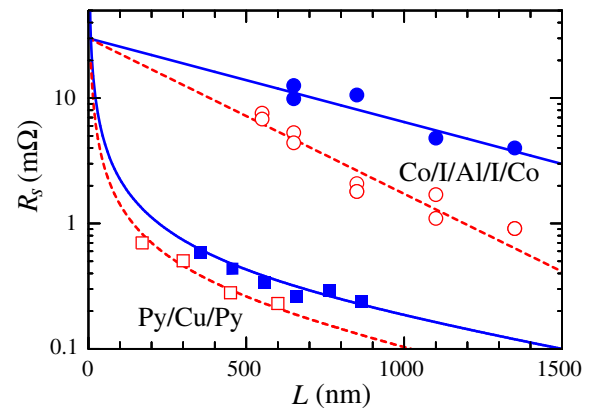


FIG. 2: Spin accumulation signal  $R_s$  as a function of distance  $L$  between the ferromagnetic electrodes in tunnel devices: ( $\bullet, \circ$ ) Co/I/Al/I/Co [4], and in metallic-contact devices: ( $\square, \blacksquare$ ) Py/Cu/Py [24, 25], where ( $\bullet, \blacksquare$ ) are the data at 4.2K and ( $\circ, \square$ ) at room temperature.

metallic-contact device. We see that  $R_s$  in a metallic contact device is smaller by one order of magnitude than  $R_s$  in a tunnel device, because of the resistance mismatch ( $R_F/R_N \ll 1$ ). Fitting Eq. (6) to the experimental data of Co/I/Al/I/Co (I=Al<sub>2</sub>O<sub>3</sub>) in Ref. [4] yields  $l_N = 650$  nm (4.2 K),  $l_N = 350$  nm (293 K),  $P_1 = 0.1$ , and  $R_N = 3 \Omega$ . Fitting Eq. (4) to the data of Py/Cu/Py in Ref. [24] at 4.2 K yields  $l_N = 920$  nm,  $R_N = 5 \Omega$ ,  $[p_F/(1-p_F^2)](R_F/R_N) = 5 \times 10^{-3}$ , and fitting to the data in Ref. [25] at 293 K yields  $l_N = 700$  nm,  $R_N = 1.75 \Omega$ , and  $[p_F/(1-p_F^2)](R_F/R_N) = 8 \times 10^{-3}$ .

The spin splitting in N in the tunneling case is

$$2\delta\mu_N(x) = P_1 e R_N I e^{-|x|/l_N}. \quad (7)$$

In the case of Co/I/Al/I/Co,  $\delta\mu_N(0) \sim 15 \mu\text{V}$  for  $P_1 \sim$

0.1,  $R_N = 3 \Omega$ , and  $I = 100 \mu\text{A}$  [4], which is much smaller than the superconducting gap  $\Delta \sim 200 \mu\text{eV}$  of an Al film.

### 3. Nonlocal spin injection and manipulation

We next study how the spin-current flow in the structure is affected by the interface condition, especially, the spin current through the N/F2 interface, because of the interest in spin-current induced magnetization switching [26].

The spin current injected nonlocally across the N/F2 interface is given by [14]

$$I_{N/F2}^{\text{spin}} = 2I \frac{\left( \frac{P_1}{1-P_1^2} \frac{R_1}{R_N} + \frac{p_F}{1-p_F^2} \frac{R_F}{R_N} \right) e^{-L/l_N}}{\left( 1 + \frac{2}{1-P_1^2} \frac{R_1}{R_N} + \frac{2}{1-p_F^2} \frac{R_F}{R_N} \right) \left( 1 + \frac{2}{1-P_2^2} \frac{R_2}{R_N} + \frac{2}{1-p_F^2} \frac{R_F}{R_N} \right) - e^{-2L/l_N}}. \quad (8)$$

A large spin-current injection occurs when junction 2 is a metallic contact ( $R_2 \ll R_N$ ) and junction 1 is a tunnel junction ( $R_1 \gg R_N$ ), yielding

$$I_{N/F2}^{\text{spin}} \approx P_1 I e^{-L/l_N}, \quad (9)$$

for F2 with very short  $l_F$ . The spin current flowing in N on the left side of F2 is  $I_N^{\text{spin}} = P_1 I e^{-x/l_N}$ , which is two times larger than that in the absence of F2, while on the right side left  $I_N^{\text{spin}} \approx 0$ . This indicates that F2 like Py and CoFe works as a strong absorber (sink) for spin current, providing a method for magnetization reversal in nonlocal devices with reduced dimensions of F2 island [27].

### 4. Spin injection into superconductors

The spin transport in a device containing a superconductor (S) such as Co/I/Al/I/Co is of great interest, because  $R_s$  is strongly influenced by opening the superconducting gap. In such tunneling device, the spin signal would be strongly affected by opening the superconducting gap  $\Delta$ .

We first show that the spin diffusion length in the superconducting state is the same as that in the normal state [28, 29]. This is intuitively understood as follows. Since the dispersion curve of the quasiparticle (QP) excitation energy is given by  $E_k = \sqrt{\xi_k^2 + \Delta^2}$  with one-electron energy  $\xi_k$  [30], the QP's velocity  $\tilde{v}_k = (1/\hbar)(\partial E_k/\partial k) = (|\xi_k|/E_k)v_k$  is slower by the factor

$|\xi_k|/E_k$  compared with the normal-state velocity  $v_k (\approx v_F)$ . By contrast, the impurity scattering time [31]  $\tilde{\tau} = (E_k/|\xi_k|)\tau$  is longer by the inverse of the factor. Then, the spin-diffusion length in S,  $l_S = (\tilde{D}\tilde{\tau}_{sf})^{1/2}$  with  $\tilde{D} = \frac{1}{3}\tilde{v}_k^2\tilde{\tau}_{tr} = (|\xi_k|/E_k)D$  turns out to be the same as  $l_N$ , owing to the cancellation of the factor  $|\xi_k|/E_k$ .

The spin accumulation in S is determined by balancing the spin injection rate with the spin-relaxation rate:

$$I_1^{\text{spin}} - I_2^{\text{spin}} + e(\partial S/\partial t)_{\text{sf}} = 0, \quad (10)$$

where  $S$  is the total spins in S, and  $I_1^{\text{spin}}$  and  $I_2^{\text{spin}}$  are the rates of incoming and outgoing spin currents through junction 1 and 2, respectively. At low temperatures the spin relaxation is dominated by spin-flip scattering via the spin-orbit interaction  $V_{\text{so}}$  at nonmagnetic impurities or grain boundaries. The scattering matrix elements of  $V_{\text{so}}$  over QP states  $|\mathbf{k}\sigma\rangle$  with momentum  $\mathbf{k}$  and spin  $\sigma$  has the form:  $\langle \mathbf{k}'\sigma' | V_{\text{so}} | \mathbf{k}\sigma \rangle = i\eta_{\text{so}}(u_{k'}u_k - v_{k'}v_k)[\vec{\sigma}'\sigma \cdot (\mathbf{k} \times \mathbf{k}')/k_{\text{F}}^2]V_{\text{imp}}$ , where  $\eta_{\text{so}}$  is the spin-orbit coupling parameter,  $V_{\text{imp}}$  is the impurity potential,  $\sigma$  is the Pauli spin matrix, and  $u_k^2 = 1 - v_k^2 = \frac{1}{2}(1 + \xi_k/E_k)$  are the coherent factors [30]. Using the golden rule for spin-flip scattering processes, we obtain the spin-relaxation rate in the form [32, 33]

$$(\partial S/\partial t)_{\text{sf}} = -S/\tau_{\text{sf}}(T), \quad (11)$$

where  $S = \chi_s(T)S_N$  with  $S_N$  the normal-state value and  $\chi_s(T)$  the QP spin-susceptibility called the Yosida func-

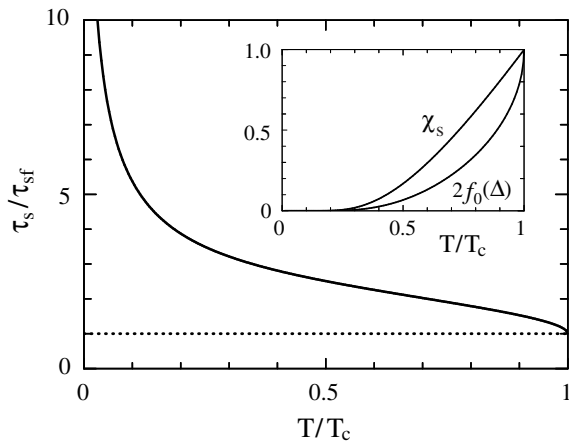


FIG. 3: Temperature dependence of the spin relaxation time  $\tau_s$  in the superconducting state. The inset shows  $\chi_s$  and  $2f_0(\Delta)$  vs.  $T$ .

tion [34], and

$$\tau_s(T) = [\chi_s(T)/2f_0(\Delta)] \tau_{sf}, \quad (12)$$

where  $\tau_{sf}$  is the spin-flip scattering time in the normal state. Equation (12) was derived earlier by Yafet [33] who studied the electron-spin resonance (ESR) in the superconducting state. Figure 3 shows the temperature dependence of  $\tau_s/\tau_{sf}$ . In the superconducting state below the superconducting critical temperature  $T_c$ ,  $\tau_s$  becomes longer with decreasing  $T$  according to  $\tau_s \simeq (\pi\Delta/2k_B T)^{1/2} \tau_{sf}$  at low temperatures.

Since the spin diffusion length in the superconducting state is the same as that in the normal state, the ECP shift in S is  $\delta\mu_S = (\tilde{a}_1 e^{-|x|/l_N} - \tilde{a}_2 e^{-|x-L|/l_N})$ , where  $\tilde{a}_i$  is calculated as follows. In the tunnel device, the tunnel spin currents are  $I_1^{\text{spin}} = P_1 I$  and  $I_2^{\text{spin}} \approx 0$ , so that Eqs (10) and (11) give the coefficients  $\tilde{a}_1 = P_1 R_N e I / [2f_0(\Delta)]$  and  $\tilde{a}_2 \approx 0$ , leading to the spin splitting of ECP in the superconducting state [14]

$$\delta\mu_S(x) = \frac{1}{2} P_1 \frac{R_N e I}{2f_0(\Delta)} e^{-|x|/l_N}, \quad (13)$$

indicating that the splitting in ECP is enhanced by the factor  $1/[2f_0(\Delta)]$  compared with the normal-state value (see Eq. 7). The detected voltage  $V_2$  by F2 at distance  $L$  is given by  $V_2 = \pm P_2 \delta\mu_S(L)$  for the P (+) and AP (-) alignments. Therefore, the spin signal  $R_s$  in the superconducting state becomes [14]

$$R_s = P_1 P_2 R_N e^{-L/l_N} / [2f_0(\Delta)]. \quad (14)$$

The above result is also obtained by the replacement  $\rho_N \rightarrow \rho_N/[2f_0(\Delta)]$  in the normal-state result of Eq. (6), which results from the fact that the QP carrier density decreases in proportion to  $2f_0(\Delta)$ , and superconductors

become a low carrier system for spin transport. The rapid increase in  $R_s$  below  $T_c$  reflects the strong reduction of the carrier population. However, when the splitting  $\delta\mu_S \sim \frac{1}{2} e P_1 R_N I / [2f_0(\Delta)]$  at  $x = 0$  becomes comparable to or larger than  $\Delta$ , the superconductivity is suppressed or destroyed by pair breaking due to the spin splitting [35, 36, 37, 38, 39, 40]. This prediction can be tested by measuring  $R_s$  in Co/I/Al/I/Co or Py/I/Al/I/Py in the superconducting state.

## 5. Spin-current induced spin Hall effect

The basic mechanism for the spin Hall effect (SHE) is the spin-orbit interaction in N, which causes a spin-asymmetry in the scattering of conduction electrons by impurities; up-spin electrons are preferentially scattered in one direction and down-spin electrons in the opposite direction. Spin injection techniques makes it possible to cause SHE in *nonmagnetic* conductors. When spin-polarized electrons are injected from a ferromagnet (F) to a nonmagnetic electrode (N), these electrons moving in N are deflected by the spin-orbit interaction to induce the Hall current in the transverse direction and accumulate charge on the sides of N [41, 42, 43].

We consider a spin-injection Hall device shown in Fig. 4. The magnetization of F electrode points to the  $z$  direction. Using the Boltzmann transport equation which incorporates the asymmetric scattering by nonmagnetic impurities, we obtain the total charge current in N [43]

$$\mathbf{j}_{\text{tot}} = \alpha_H [\hat{\mathbf{z}} \times \mathbf{j}_{\text{spin}}] + \sigma_N \mathbf{E}, \quad (15)$$

where the first term is the Hall current  $\mathbf{j}_H$  induced by the spin current, the second term is the Ohmic current,  $\mathbf{E}$  is the electric field induced by surface charge, and  $\alpha_H \sim \eta_{\text{so}} N(0) V_{\text{imp}}$  (skew scattering). In the open circuit condition in the transverse direction, the  $y$  component of  $\mathbf{j}_{\text{tot}}$  vanishes, so that the nonlocal Hall resistance

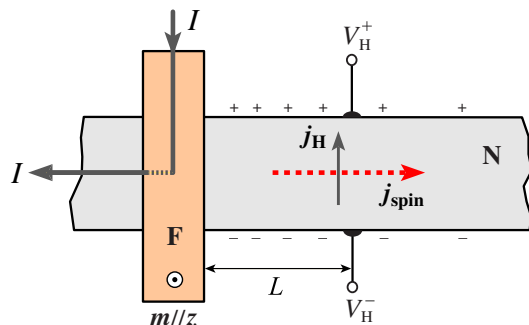


FIG. 4: Spin injection Hall device (top view). The magnetic moment of F is aligned perpendicular to the plane. The anomalous Hall voltage  $V_H = V_H^+ - V_H^-$  is induced in the transverse direction by injection of spin-polarized current.

TABLE I: Spin-orbit coupling parameter of Cu and Al.

	$l_N$ (nm)	$\rho_N$ ( $\mu\Omega\text{cm}$ )	$\tau_{\text{imp}}/\tau_{\text{sf}}$	$\eta_{\text{so}}$
Cu	1000 <sup>a</sup>	1.43 <sup>a</sup>	$0.70 \times 10^{-3}$	0.040
Cu	546 <sup>b</sup>	3.44 <sup>b</sup>	$0.41 \times 10^{-3}$	0.030
Al	650 <sup>c</sup>	5.90 <sup>c</sup>	$0.36 \times 10^{-4}$	0.009
Al	705 <sup>d</sup>	5.88 <sup>d</sup>	$0.30 \times 10^{-4}$	0.008
Ag	195 <sup>e</sup>	3.50 <sup>e</sup>	$0.50 \times 10^{-2}$	0.110

<sup>a</sup>Ref. [3], <sup>b</sup>Ref. [8], <sup>c</sup>Ref. [4], <sup>d</sup>Ref. [45], <sup>e</sup>Ref. [10].

$R_H = V_H/I$  becomes

$$R_H = \frac{1}{2} (P_1 \alpha_H \rho_N / d_N) e^{-L/l_N}, \quad (16)$$

in the tunneling case. Recently, SHE induced by the spin-current have been measured in a Py/Cu structure using the spin injection technique [44, 45, 46].

It is noteworthy that the product  $\rho_N l_N$  is related to the spin-orbit coupling parameter  $\eta_{\text{so}}$  as [48]

$$\rho_N l_N = \frac{\sqrt{3}\pi R_K}{2 k_F^2} \sqrt{\frac{\tau_{\text{sf}}}{\tau_{\text{imp}}}} = \frac{3\sqrt{3}\pi R_K}{4 k_F^2} \frac{1}{\eta_{\text{so}}}, \quad (17)$$

where  $R_K = h/e^2 \sim 25.8 \text{ k}\Omega$  is the quantum resistance. The formula (17) provides a method for obtaining information for spin-orbit scattering in nonmagnetic metals. Using the experimental data of  $\rho_N$  and  $l_N$  and the Fermi momentum  $k_F$  [49] in Eq. (17), we obtain the value of the spin-orbit coupling parameter  $\eta_{\text{so}} = 0.01\text{--}0.04$  in Cu and Al as listed in Table 1. Therefore, Eq. (16) yields  $R_H$  of the order of  $1 \text{ m}\Omega$ , indicating that the spin-current induced SHE is observable by using the nonlocal geometry.

## Acknowledgement

The authors thank M. Ichimura, H. Imamura, and T. Yamashita for valuable discussions. This work is supported by a Grant-in-Aid for Scientific Research from MEXT and the NAREGI Nanoscience Project.

- 
- [1] *Concept in Spin Electronics*, edited by S. Maekawa (Oxford Univ Press, 2006).  
 [2] M. Johnson and R.H. Silsbee, Phys. Rev. Lett. **55**, 1790 (1985); *ibid.* **60**, 377 (1988); M. Johnson, *ibid.* **70**, 2142 (1993).  
 [3] F. J. Jedema, A. T. Filip and B. J. van Wees, Nature (London) **410**, 345 (2001)  
 [4] F. J. Jedema, H. B. Heersche, A. T. Filip, J. J. A. Baselmans, and B. J. van Wees, Nature (London) **416**, 713 (2002).  
 [5] T. Kimura, J. Hamrle, Y. Otani, K. Tsukagoshi, and Y. Aoyagi, Appl. Phys. Lett. **85**, 3795 (2004); T. Kimura, J. Hamrle, Y. Otani, Phys. Rev. B **72**, 14461 (2005).

- [6] M. Urech, J. Johansson, V. Korenivski and D. B. Haviland, J. Magn. Magn. Mater. **272-276**, E1469 (2004).  
 [7] Y. Ji, A. Hoffmann, J. S. Jiang, and S. D. Bader, Appl. Phys. Lett. **85**, 6218 (2004).  
 [8] S. Garzon, I. Žutić, and R. A. Webb, Phys. Rev. Lett. **94**, 176601 (2005).  
 [9] K. Miura, T. Ono, S. Nasu, T. Okuno, K. Mibu, and T. Shinjo, J. Magn. Magn. Mater. **286**, 142 (2005).  
 [10] R. Godfrey and M. Johnson, Phys. Rev. Lett. **96** (2006) 136601.  
 [11] T. Valet and A. Fert, Phys. Rev. B **48**, 7099 (1993).  
 [12] A. Fert and S.F. Lee, Phys. Rev. B **53**, 6554 (1996).  
 [13] S. Hershfield and H.L. Zhao, Phys. Rev. B **56**, 3296 (1997).  
 [14] S. Takahashi and S. Maekawa, Phys. Rev. B **67**, 052409 (2003).  
 [15] J. Bass and W.P. Pratt Jr., J. Magn. and Magn. Mater. **200** (1999) 274.  
 [16] M. Ichimura, S. Takahashi, K. Ito, and S. Maekawa, J. Appl. Phys. **95**, 7225 (2004).  
 [17] J. Hamrle, T. Kimura, T. Yang, and Y. Otani, Phys. Rev. B **71**, 094434 (2005).  
 [18] R. J. Soulen Jr. *et al.*, Science **282**, 85 (1998).  
 [19] R. Meservey and P. M. Tedrow, Phys. Rep. **238**, 173 (1994).  
 [20] J. S. Moodera and G. Mathon, J. Magn. Magn. Mater. **200**, 248 (1999).  
 [21] D. J. Monsma and S. S. P. Parkin, Appl. Phys. Lett. **77**, 720 (2000).  
 [22] S. S. P. Parkin *et al* Nature Materials **3**, 862 (2004).  
 [23] S. Yuasa, T. Nagahama, A. Fukushima, Y. Suzuki, and K. Ando, Nature Materials **3**, 868 (2004).  
 [24] S. Garzon, Ph.D. Thesis (Univ. Maryland, 2005).  
 [25] T. Kimura, J. Hamrle, and Y. Otani, J. Magn. Soc. Jpn. **29**, 192 (2005).  
 [26] J. C. Slonczewski, J. Mag. Mag. Mater. **159**, L1 (1996).  
 [27] T. Kimura, Y. Otani, and J. Hamrle, Phys. Re. Lett. **96**, 037201 (2006). In their device of Py/Cu/Py, the junctions are both metallic contact, so that  $I_{N/F2}^{\text{spin}} \approx [p_F/(1-p_F^2)]I(R_F/R_N) \sinh^{-1}(L/l_N)$ .  
 [28] T. Yamashita, S. Takahashi, H. Imamura, and S. Maekawa, Phys. Rev. B **65**, 172509 (2002).  
 [29] J. P. Morten, A. Brataas, and W. Belzig [Phys. Rev. B **70**, 212508 (2004)] have pointed out that, in the *elastic* transport regime, the spin-diffusion length is renormalized in the superconducting state.  
 [30] M. Tinkham, *Introduction to Superconductivity* (McGraw-Hill, New York, 1996).  
 [31] J. Bardeen, G. Rickayzen, and L. Tewordt, Phys. Rev. **113**, 982 (1959).  
 [32] S. Takahashi, T. Yamashita, H. Imamura, S. Maekawa, J. Magn. Magn. Mater. **240**, 100 (2002).  
 [33] Y. Yafet, Phys. Lett. **98**, 287 (1983).  
 [34] K. Yosida, Phys. Rev. **110**, 769 (1958).  
 [35] S. Takahashi, H. Imamura, and S. Maekawa, Phys. Rev. Lett. **82**, 3911 (1999).  
 [36] S. Takahashi, H. Imamura, and S. Maekawa, J. Appl. Phys. **85**, 5227 (2000); Physica C **341-348**, 1515 (2000).  
 [37] C. D. Chen, Watson Kuo, D. S. Chung, J. H. Shyu, and C. S. Wu, Phys. Rev. Lett. **88**, 047004 (2002).  
 [38] J. Johansson, M. Urech, D. Haviland, and V. Korenivski, J. Appl. Phys. **93**, 8650 (2003).  
 [39] D. Wang and J. G. Lu, J. Appl. Phys. **97**, 10A708 (2005).

- [40] T. Daibou, M. Oogane, Y. Ando, and T. Miyazaki, (unpublished).
- [41] J. E. Hirsch, Phys. Rev. Lett. **83** (1999) 1834.
- [42] S. Zhang, Phys. Rev. Lett. **85** (2001) 393.
- [43] S. Takahashi and S. Maekawa, Phys. Rev. Lett. **88**, 116601 (2002).
- [44] T. Kimura, Y. Otani, K. Tsukagoshi and Y. Aoyagi, J. Magn. Magn. Mater. **272-276**, e1333 (2004).
- [45] S. O. Valenzuela and M. Tinkham, Nature **442**, 176 (2006).
- [46] T. Kimura, Y. Otani, T. Sato, S. Takahashi, and S. Maekawa, cond-mat/0609304.
- [47] F. J. Jedema, M. S. Nijboer, A. T. Filip, and B. J. van Wees, Phys. Rev. B **67**, 085319 (2003).
- [48] S. Takahashi, H. Imamura, and S. Maekawa, Chapter 8 in *Concept in Spin Electronics*, edited by S. Maekawa (Oxford Univ Press, 2006).
- [49] N. W. Ashcroft and D. Mermin, *Solid State Physics*, (Saunders College, 1976).